Ensemble-Based Analysis of Errors in Atmospheric Profiles Retrieved from GNSS Occultation Data
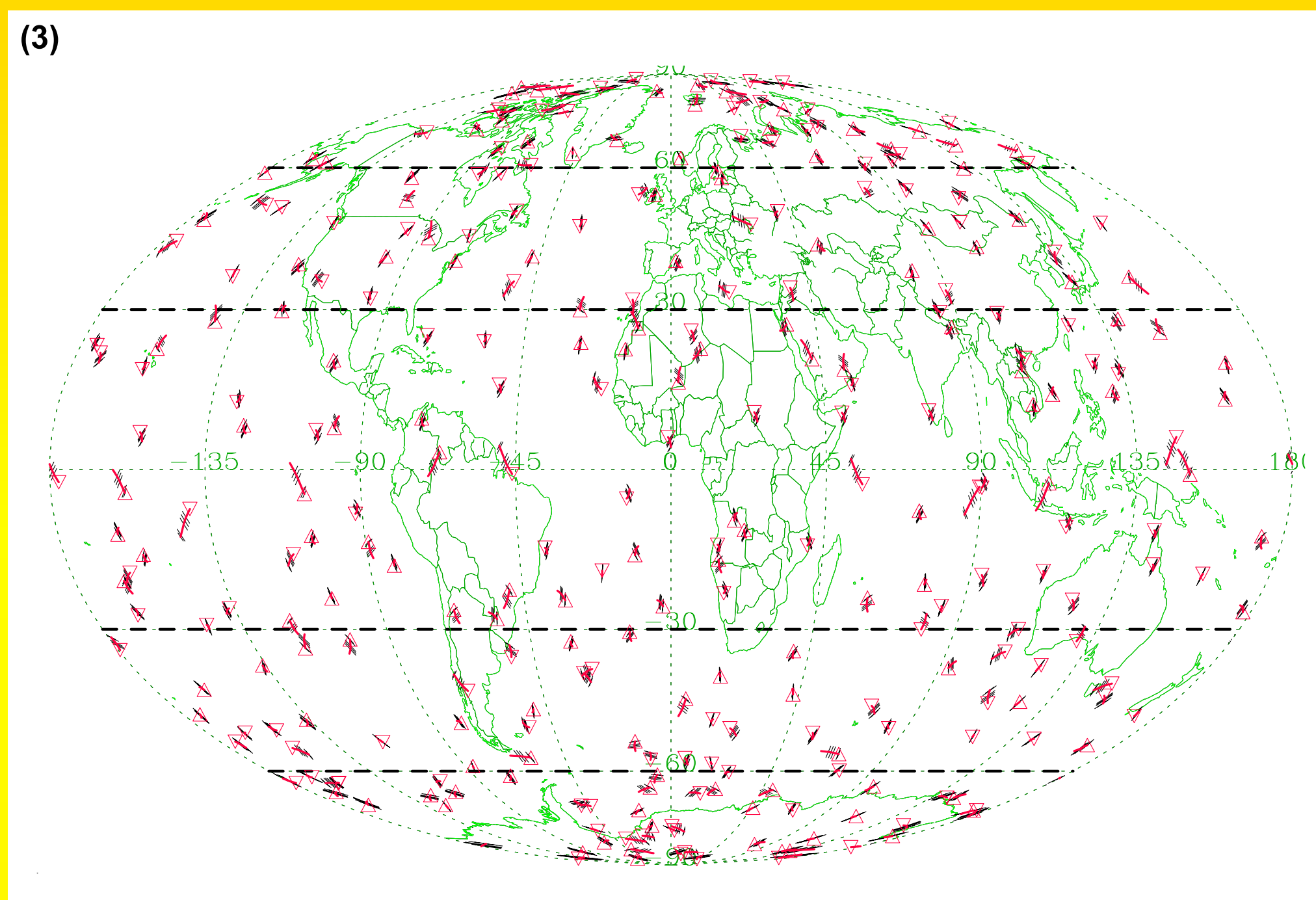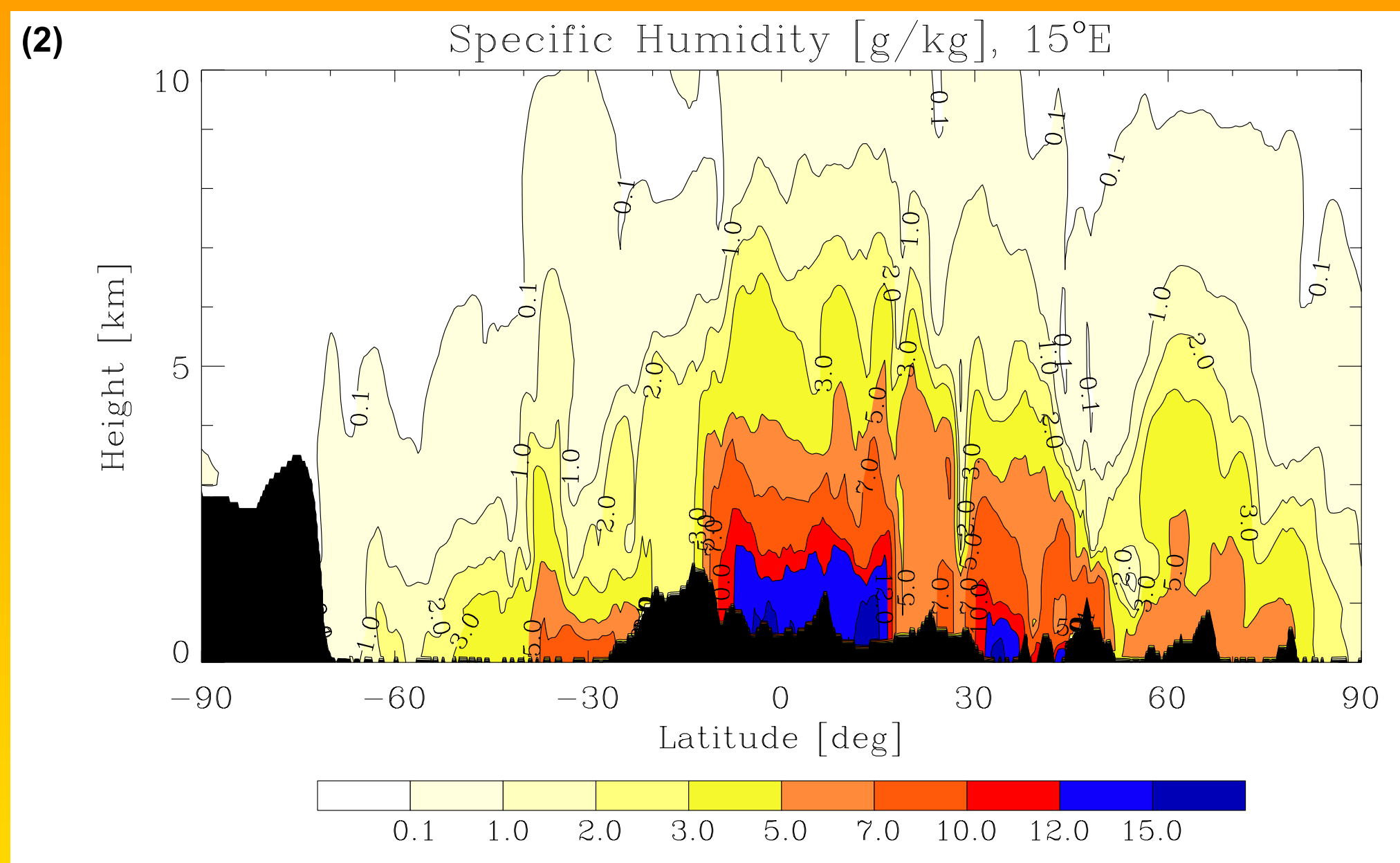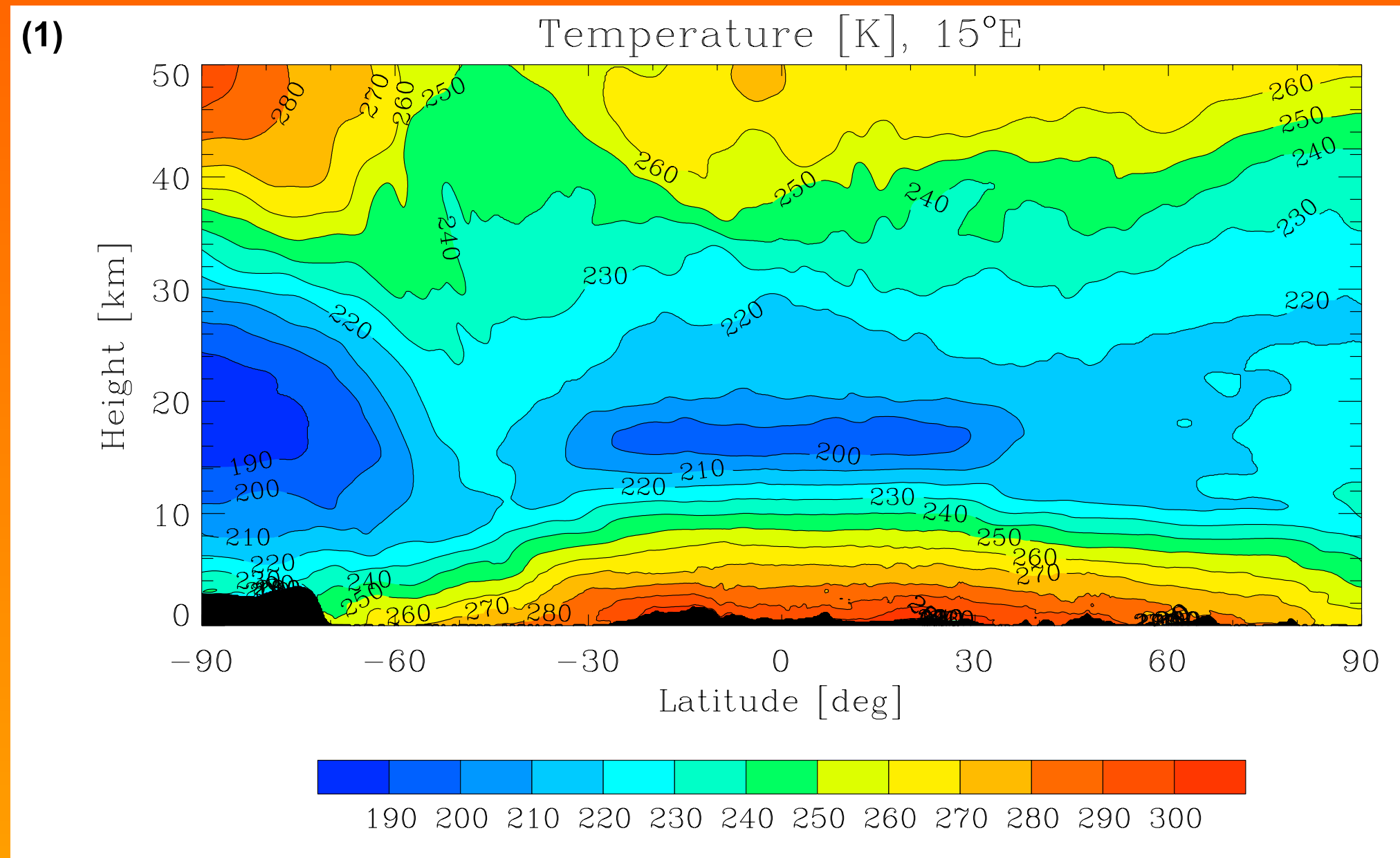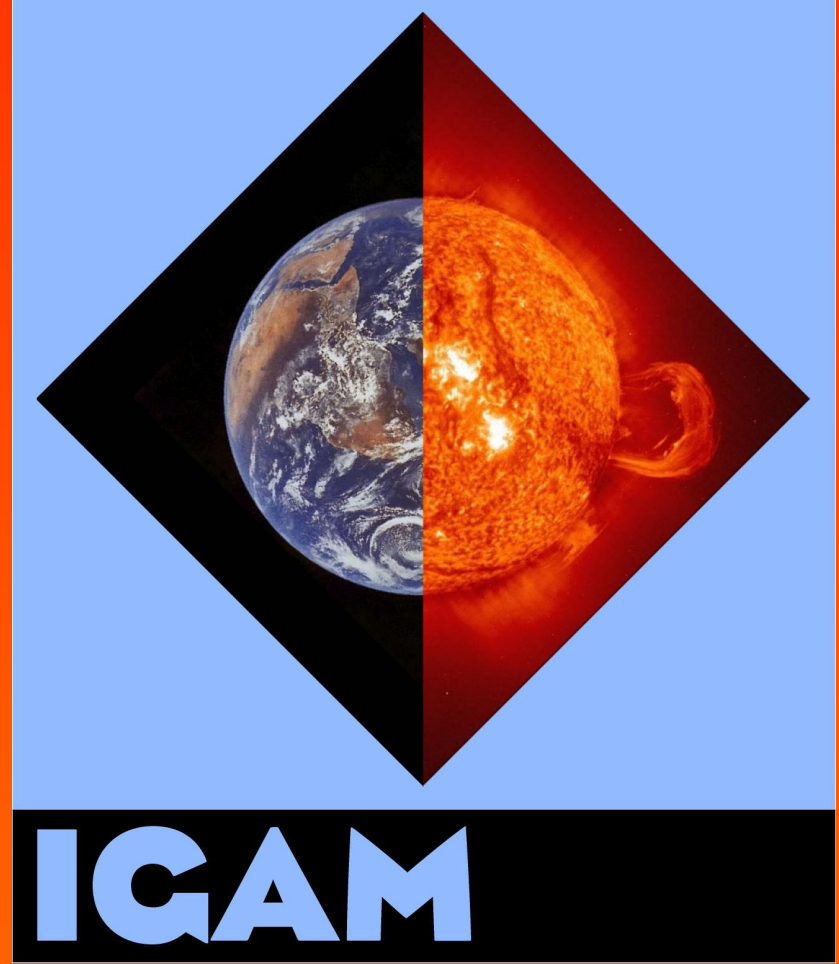
Andrea K. Steiner and Gottfried Kirchengast
(andi.steiner@uni-graz.at, gottfried.kirchengast@uni-graz.at)
Institute for Geophysics, Astrophysics, and Meteorology (IGAM), University of Graz, Austria

IGAM

UNI GRAZ

(1) Introduction

Radio occultation observations using the Global Navigation Satellite System (GNSS) provide high quality atmospheric data to improve climate monitoring and modeling as well as numerical weather prediction and analysis. In order to obtain realistic information on the errors of GNSS retrieval products (e.g., for data assimilation systems) we performed an empirical error analysis based on realistically simulated data.

(2) Ensemble Design and Simulations

We simulated a suitable dataset with the End-to-end GNSS Occultation Performance Simulator (EGOPS; details: www.uni-graz.at/igam-iemc) involving realistic atmospheric profiles and error characteristics. A T213L50 ECMWF analysis field with the highest model level at 0.1 hPa was used as atmospheric model input (Figures 1 and 2). The ionosphere was prescribed with the NeUoG model, a global empirical 3D climatological model of the ionospheric electron density field. Observations were simulated for one day, September 15, 1999, adopting the planned European Meteorological Operational satellite (METOP) as Low Earth Orbit (LEO) satellite and its GNSS Receiver for Atmospheric Sounding (GRAS) as sensor. We chose an ensemble of 300 events out of 574 in total, which are equally distributed in time and space with 100 events in each of three (low-mid-high) latitude bands (Fig. 3).

(1) Temperature [K], 15°E

(2) Specific Humidity [g/kg], 15°E

(3)

(3) Phase and Doppler Observables

Forward modeling of the signal propagation through the atmosphere-ionosphere system was performed with a sub-millimetric precision 3D ray tracer. Observation system simulation, including instrument and raw processing errors, provided realistic excess phase paths. Figure 4 (left panels a–d) shows the ionosphere-corrected phase path delays LC. An occultation event lasts 1–2 min with a (neutral-gas) delay of ~2 mm near the mesopause (~80 km $\hat{=}$ ~4 sec; also ionospheric residuals involved), ~20 cm near the stratopause (~50 km $\hat{=}$ ~16 sec), and >20 m below tropopause levels (~15 km $\hat{=}$ ~30 sec). The near-surface delay reaches ~0.7–2 km depending on the water vapor content. The rms error of the LC phase sampled at 10 Hz is found to be 2–3 mm at <30 sec (Fig. 4, middle panels), which well and conservatively reflects METOP/GRAS receiving system performance. While absolute errors increase into the troposphere, relative rms errors are found to be <0.02% at these low heights. The time derivative of phase, the Doppler shift, shows a reasonable rms error of near 3 mm/sec (Fig. 4, right panels). Also for the Doppler shift, relative errors do not exceed ~0.01% in the troposphere. Biases in both, phase delay and Doppler shift, are negligible, reflecting the self-calibrated nature of these basic observables.

(4)
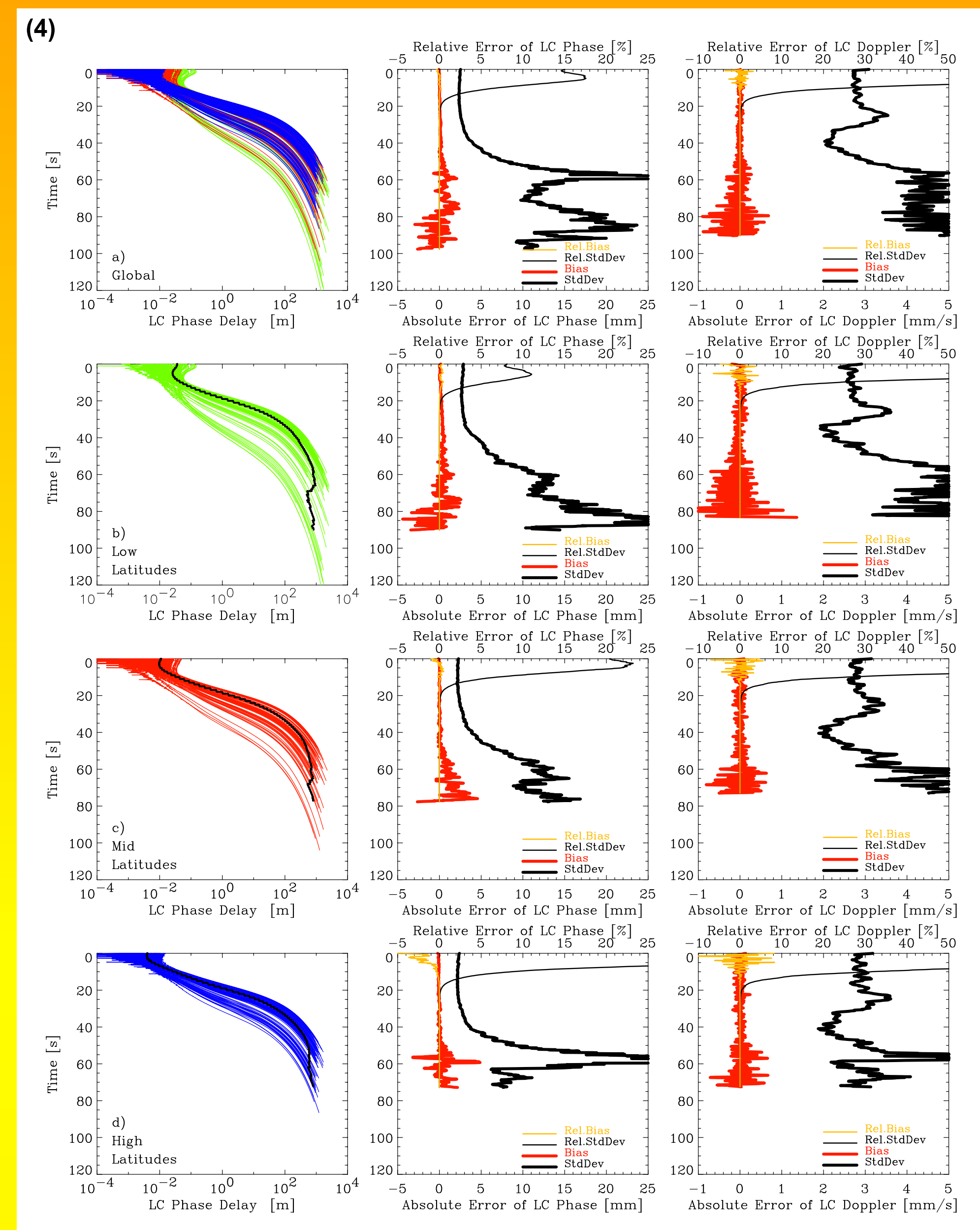
(4) Error Analysis Scheme

Atmospheric profiles of bending angle, refractivity (N), pressure, geopotential height, temperature (T), and humidity (q) were retrieved with a state-of-the-art data processing chain involving inverse-covariance-weighted statistical optimization of measured bending angles and best-fit MSIS90 model bending angles. In the troposphere, an optimal estimation retrieval was applied to N using the ECMWF 24-hour short-range forecast as background field for T and q. The difference $\Delta\mathbf{x}$ of the retrieved profiles $\mathbf{x}^{retr}$ and the "true" co-located profiles $\mathbf{x}^{true}$ was computed at an ECMWF-type L60 vertical grid. Errors were analyzed for each retrieval product, yielding realistic bias profiles $\mathbf{b}$ and covariance matrices $\mathbf{S}$, as well as the derived quantities $\mathbf{s}$ and $\mathbf{R}$.

- Difference profiles: $\Delta\mathbf{x} = \left(\mathbf{x}^{retr} - \mathbf{x}^{true}\right)$
- Bias: $\mathbf{b} = \left[\frac{1}{N}\sum\left(\Delta\mathbf{x}_k\right)\right], k = 1, \textit{No. of events}$
- Bias-free profiles: $\Delta\mathbf{x}^{biasfree} = \Delta\mathbf{x} - \mathbf{b}$
- Error Covariance Matrix: $\mathbf{S} = \left[\frac{1}{N-1}\sum\left(\Delta\mathbf{x}_k^{biasfree}\right)\left(\Delta\mathbf{x}_k^{biasfree}\right)^T\right]$
- Standard Deviation: $\mathbf{s} = \sqrt{S_{ii}}$
- Correlation Matrix: $\mathbf{R} \text{ with } R_{ij} = \frac{S_{ij}}{\sqrt{S_{ii}S_{jj}}}$

(5) Results

We present, as examples, refractivity (Fig. 5) and temperature (Fig. 6) error analysis results for global and latitudinal data sets (a–d); middle panels show bias, standard deviation (stddev) and rms, right panels show correlation functions (corrfs). Refractivity exhibits a relative stddev of 0.1–0.75% at 5–40 km height and a relative bias of <0.1% in this "core" domain (global). Temperature shows a stddev of 0.2–1 K at 3–31 km height and a bias of <0.5 K below 33 km and of <0.1 K below 20 km (global). The temperature bias is lowest at mid latitudes with <0.2 K at 2–40 km and largest at high latitudes with >3 K above 40 km (due to inadequate a priori profiles in this region). Fig. 7 shows corrfs for representative height levels, denoting the correlation of errors at these heights with those in the remainder of the profile. Bending angle corrfs are sharp, whilst refractivity corrfs are broader due to the effect of Abelian integration. Pressure and geopotential height errors are strongly correlated due to hydrostatic integration. Temperature corrfs are most akin to refractivity corrfs again, and humidity errors also show distinct correlation. *Rieder and Kirchengast* (*JGR* **106**, 31755-31770, 2001) provided some theoretical background on these properties. This empirical study now led to realistic error estimates, including biases, which are a valuable basis for further retrieval algorithm improvements and for proper specification of observational errors in data assimilation systems.

(5)

(6)

(7)